Chemical Geology 291 (2012) 55–68

Contents lists available at SciVerse ScienceDirect

Chemical Geology

journal homepage: www.elsevier.com/locate/chemgeo

Research paper

Chemistry, microstructure, and alpha decay damage of natural brannerite

G.R. Lumpkin *, S.H.F. Leung, J. Ferenczy

Materials Division, Australian Nuclear Science and Technology Organisation, Private Mail Bag 1, Menai, NSW 2234, Australia

ARTICLE INFO

Article history:
Received 13 June 2011
Accepted 13 September 2011
Available online 17 September 2011

Editor: D.B. Dingwell

Keywords:
Alpha decay damage
Alpine pegmatites
Brannerite
Crocker's Well, South Australia
Geochemical alteration
U–Th–Pb age dating

ABSTRACT

To investigate the long-term stability of brannerite with respect to alpha decay damage and interaction with aqueous fluids, we have undertaken a study of twelve natural samples from a range of geological environments. Our results indicate that seven of the samples exhibit only minor alteration, usually located within veinlets or around the rim of the sample. The remaining five samples consist of variable amounts of unaltered and altered brannerite. Based on a total of 3 metal cations, the Ti and U contents of unaltered brannerite range from 1.8 to 2.1 and 0.4 to 0.9 atoms per formula unit (apfu), respectively. Maximum amounts of the other major cations on the A-site are 0.48 Ca, 0.22 Th, 0.14 Y, and 0.07 Ln (lanthanide = Ce, Nd, Gd, Sm) atoms pfu. Maximum values of other cations on the B-site are 0.15 Fe, 0.14 Si, 0.09 Al, 0.06 Nb, 0.04 Mn, and 0.04 Ni atoms pfu. Altered regions of brannerite contain significant amounts of Si and other elements incorporated from an aqueous fluid phase, and up to 40–90% of the original amount of U has been lost as a result of alteration. SEM-EDX results also provide evidence for TiO_2 phases, galena, and a thorite-like phase as alteration products. Electron diffraction patterns of all samples typically consist of two broad, diffuse rings that have equivalent d-spacings of 0.31 nm and 0.19 nm, indicating that brannerite is rendered completely amorphous by alpha decay damage. Many of the grains also exhibit weak diffraction spots due to fine-grained inclusions of a uranium oxide phase and galena. Using the available age data, these samples have accumulated alpha decay doses in the range of $0.7–200 \times 10^{16}$ α mg^{-1}. Although imprecise, the U–Th–Pb chemical ages determined by microanalysis are generally consistent with the known ages and geological histories of the brannerite host rocks. To a first approximation, it is possible to understand the results of chemical and isotopic dating of brannerite by treating each sample as a complex system composed of nominally unaltered, altered, and recrystallised areas. The dominant effects are U loss from altered areas and Pb loss from unaltered brannerite and, to a lesser extent, altered brannerite, the structure of which approximates to a Ti–Si–O glass-like network wherein Pb is more comfortable as a network modifier.

1. Introduction

Brannerite, ideally UTi_2O_6, is a common accessory phase in special purpose, pyrochlore-rich titanate ceramics designed for the encapsulation of actinide-rich nuclear wastes. In particular, the pyrochlore-rich waste forms are candidates for the long-term storage of surplus Pu in the United States, Russia, and the United Kingdom. Designs in the United States, circa 2000, called for ceramic pucks containing about 35–40 wt.% TiO_2, 20–25 wt.% UO_2, 10 wt.% PuO_2, 10 wt.% HfO_2, 7–10 wt.% Gd_2O_3, and 8–12 wt.% CaO. These ceramic materials typically contain 60–90% pyrochlore (ideally $CaUTi_2O_7$), 0–25% zirconolite (ideally $CaZrTi_2O_7$), 0–20% brannerite, and 0–15% rutile (ideally TiO_2). Zirconolite-rich ceramics have also been produced from the basic formulation by increasing the Hf content at the expense of U. Extensive work has been carried out on these waste forms and related ceramic materials in terms of processing parameters, phase assemblages, incorporation of minor elements, and overall element partitioning with the general aim of producing bulk ceramics with minimal degradation of physical properties (e.g., bulk swelling and cracking) and high chemical durability in aqueous fluids following extensive radiation damage (Strachan et al., 2005; Icenhower et al., 2006; Strachan et al., 2008).

The aqueous dissolution kinetics of nearly single phase samples of pyrochlore, zirconolite, and brannerite have been determined as a function of temperature and pH (Roberts et al., 2000; Zhang et al., 2001). Results of these studies demonstrate that the dissolution rates of all three phases exhibit a shallow v-shaped pattern as a function of pH with a minimum at pH = 8 at temperatures of 25–75 °C. Minimum dissolution rates are typically between 10^{-6} and 10^{-5} g m^{-2} d^{-1} at pH = 8 and maximum values are between 10^{-6} and 10^{-5} g m^{-2} d^{-1} at pH = 2. Dissolution rates generally follow the order brannerite > pyrochlore > zirconolite, especially at low pH values. In general, the dissolution of brannerite is non-stoichiometric as a function of pH, with enhanced release of U relative to Ti under acidic conditions (Zhang et al., 2003). Thomas and Zhang (2003) provided a kinetic model of the oxidative dissolution of brannerite based

* Corresponding author. Tel.: +61 2 9717 3475; fax: +61 2 9543 7179.
E-mail addresses: grl@ansto.gov.au, g_lumpkin@hotmail.com (G.R. Lumpkin).

0009-2541/$ – see front matter.
doi:10.1016/j.chemgeo.2011.09.008

on the oxidation of surface U^{4+} atoms followed by release of U^{6+} to solution, driven by protons or carbonate species under acidic or alkaline conditions, respectively. A kinetic rate law using this simple two-step model was shown to provide a qualitative description of the pH dependence of the dissolution of brannerite over a range of pH.

Even though brannerite is a minor phase in these pyrochlore-rich waste forms, the pure end-member composition contains 62.8 wt.% UO_2; therefore, it may account for a significant fraction of the total amount of actinides in the bulk solid. In order to study both the short-term and the long-term behavior of brannerite, it is sometimes useful to employ a combination of laboratory experiments and natural analog studies. As in previous investigations of natural samples, these studies are designed to assess both the aqueous durability and radiation damage effects. In this report, we provide results on the chemistry and microstructure of a suite of twelve brannerite samples from several different localities, ranging in age from about 5 Ma to 1.6 Ga. The geological environments of these samples are granitic rocks, pegmatites, quartz veins, and low to medium temperature hydrothermal ore deposits. We have not included brannerite samples from low temperature, Precambrian quartz-pebble conglomerates in this study (e.g., Ferris and Ruud, 1971; Saager and Stupp, 1983). The major objectives are to assess the level chemical substitution in brannerite; describe the geochemical alteration; including the extent of U loss, elemental exchange with crustal fluids; and to determine radiation damage response as a function of age. In addition, we discuss some of the implications of U-Pb chemical ages in the context of existing geochronological information. The results of this study are compared with existing data for other potential actinide host phases, among which pyrochlore and zirconolite are particularly important in ceramic nuclear waste forms.

2. Experimental procedures

2.1. Scanning electron microscopy

SEM-EDX work was carried out on polished sections using a JEOL JSM-6400 SEM operated at 25 kV for microanalysis and 15 kV for secondary (SE) and backscattered electron (BSE) imaging. The SEM is equipped with a Noran Voyager Si(Li) microanalysis system, including an ultra-thin window detector with a nominal resolution of 134 eV on the Mn Kα X-ray peak. EDX spectra were acquired for 500 s and processed using Noran software for standardless analysis. The results are therefore normalized to 100 wt.% as part of the iterative data reduction routine (including full matrix corrections for absorption and fluorescence). However, this procedure has been optimized for the quantitative analysis of anhydrous materials by adjusting the calibration factors using a large suite of natural and synthetic reference standards. In this study, EDX spectra were obtained from unaltered brannerite, altered brannerite (identified by darker BSE contrast), and associated mineral inclusions or alteration products.

2.2. Transmission electron microscopy

TEM was performed on crushed fragments dispersed on holey carbon grids using a JEOL 2000FXII TEM equipped with a Link ISIS Si(Li) microanalysis system and operated at 200 kV. The EDX detector is of the ultra-thin window type and has a nominal resolution of 129 eV on the Mn Kα X-ray peak. The instrument was calibrated for selected area diffraction (SAED) work over a range of objective lens currents with a gold standard. The chemistry of the brannerite fragments and mineral inclusions were checked by EDX using a nominal probe size of approximately 20 nm. Spectra were acquired for 600–900 s live time (plus 20–30% dead time) and processed with the Link ISIS software package TEMQuant using previously established operation and calibration procedures (Lumpkin et al., 1994a, 1994b).

2.3. SRIM simulations

In order to provide an estimate for the number of atoms displaced per alpha decay event, N_d, in brannerite, we used the calculated density of 6.37 g cm^{-3} and two additional density values of 5.73 g cm^{-3} (10% lower) and 5.10 g cm^{-3} (20% lower) in an effort to account for the effects of hydration and radiation damage induced swelling. We conducted SRIM (the Stopping and Range of Ions in Matter; Ziegler et al., 2009) simulations as a function of density with full damage cascades in order to approximate the number of displacements for the recoil nucleus, assumed to be ^{234}U with a nominal energy of 80 keV. We also conducted additional simulations in "light ion mode" for the alpha particle by using ^{4}He and a nominal energy of 4.5 MeV. Displacement energies (E_d) were constrained to be equal for U, Ti, and O in all calculations, but due to the lack of experimental data, the calculations were performed with $E_d = 25$, 50, and 100 eV in order to further assess the range of atomic displacements produced. All binding energies (E_b) were set to the default value 3 eV for these calculations.

2.4. Alpha decay dose, displacements per atom, and age calculations

The U–Th–Pb chemical ages of the brannerite samples were calculated using the equivalent uranium (eU) method. In this approach, the present amount of ^{232}Th is converted to an equivalent amount of ^{238}U from the relationship:

$$eU = (\lambda_{238}/\lambda_{232} \times Th) + U \tag{1}$$

The age, alpha decay dose, and displacements per atom (dpa) are then obtained from Eqs. (2)–(4), respectively:

$$t = \left(e^{Pb/eU} - 1\right)/\lambda_{238} \tag{2}$$

$$D = 8N_{238}\left(e^{\lambda_{238}t} - 1\right) + 6N_{232}\left(e^{\lambda_{232}t} - 1\right) \tag{3}$$

$$dpa = (N_d \times D \times M_{bran})/\left(N_f \times N_A\right) \tag{4}$$

In these equations, λ_{238}, λ_{232}, N_{238}, and N_{232} are the decay constants and present amounts of ^{238}U and ^{232}Th per mg, M_{bran} is the molecular weight of brannerite, N_f is the number of atoms per formula unit, and N_A is Avogadro's number. In these calculations we have ignored the very small contribution from natural ^{235}U and furthermore we assume that all Pb detected by SEM-EDX is radiogenic in origin.

3. Geological background

The samples used in this study occur in a variety of geological environments and may have been exposed to late stage hydrothermal and meteoric aqueous fluids. Here we briefly summarize the localities listed in Table 1 beginning with the (nominally) oldest samples and ending with the youngest. The oldest samples in our collection are from Crocker's Well, South Australia. In this case, the host rocks have a well-defined age of 1580 Ma based on U–Th–Pb isotopic age dating of zircon (Ludwig and Cooper, 1984). Brannerite samples from Crocker's Well, South Australia, are associated with late tectonic granitoid intrusions containing plagioclase, quartz, and K-feldspar as major constituents. Here, the brannerite occurs as an accessory mineral in the granitic rocks, particularly in shear zones and fractures, and is usually associated with rutile (Campana and King, 1958; Ludwig and Cooper, 1984). The thermal history of this geological terrain is not simple, as the rocks were subjected to amphibolite grade regional metamorphism during the Early Ordovician geological time period (~420–480 Ma) as indicated by Rb-Sr isotopic dating.

Brannerite from the Kansanshi mine, Western Province, Zambia, is found in association with a low temperature Cu–Au deposit hosted

Table 1
Summary of localities, age data, and alpha decay doses of natural brannerite.

Locality	Samples	t (Ma)	t (Ma) U–Th–Pb	D (10^{16} α mg^{-1})	dpa
Crocker's Well, SA	B1, 5, 6	1580	350–680	177–200	91–104
W. Province, Zambia	B4	500–520	465	63–67	32–35
Sierra Albarrana, Spain	B2, 10	350–390	360–480	48–57	25–30
Bou-Azzer, Morocco	B8	305–315	191	42–44	21–23
San Bernardino Co., CA	B7	65–250	178	7–28	3–15
Stanley, Idaho	B11	65–90	72	8–11	4.3–5.4
Ticino, Switzerland	B3, 9, 12	20–25	≤22–29	3.0–3.8	1.5–2.0
Bourg d'Oisans, France	B13	5–11	≤25	0.7–1.6	0.3–0.8
Binntal, Switzerland[a]	–	11	–	1.3–1.6	0.7–0.9

[a] Graeser and Guggenheim (1990).

within metamorphosed (greenschist facies) and hydrothermally alered sedimentary rocks in the "Domes" region of the central African copperbelt (Kampunzu et al., 2009). The sulfide mineralization occurs within veins and is also present as finely disseminated grains in the upper part of the Katanga Supergroup. Minerals of the deposit include pyrite, pyrrhotite, chalcopyrite, and bornite together with minor amounts of monazite, brannerite, molybdenite, silver, and gold. Re–Os isotopic dating of molybdenite and U–Pb isotopic SHRIMP dating of monazite indicate that the veins have ages of approximately 500–520 Ma considering the reported uncertainties in the data (Torrealday et al., 2000).

Granitic pegmatites are also the source of brannerite in the Sierra Albarrana region of Spain (Perez et al., 1991). The pegmatites occur within lower Paleozoic metamorphic rocks, mainly gneisses, banded migmatites, and schists, and consist mainly of feldspars, micas, quartz, tourmaline, fluorapatite, and garnet. Brannerite is generally associated with quartz in the internal zones of the pegmatite dikes and may be altered to anatase and sphene. Numerous mineral specimens have come from this area, consisting of large brannerite single crystals completely enveloped by a tan alteration rind. Accessory minerals in these pegmatites include beryl, chrysoberyl, uraninite, monazite, xenotime, allanite, zircon, and columbite group minerals. The pegmatites are believed to have formed during Hercynian deformation and low-pressure metamorphism (up to amphibolite grade), suggesting an age range of approximately 350–390 Ma (Abad-Ortega et al., 1993; Azor and Ballèvre, 1997; Simancas et al., 2000).

The brannerite specimen from Bou Azzer, Morocco, also comes from a unique Co–Ni ore deposit associated with late Proterozoic ophiolite (serpentinized mantle peridotite). Most of the ore is structurally controlled and occurs primarily within quartz-carbonate-sulfide veins. The main sulfide minerals include bornite, chalcocite, chalcopyrite, pyrite, pyrrhotite, sphalerite, and tetrahedrite, together with arsenopyrite and the principle ore minerals which include a suite of Co–Ni–Fe arsenides and Au-Ag alloys (Leblanc and Billaud, 1982; Favreau et al., 2007; Ahmed et al., 2009). The tectonic history of the region is complex and the origin of the ore bodies is a subject of considerable interest and debate. Recent isotopic age dates Re-Os ages of 350–400 Ma for molybenite (Re-Os), 308 ± 31 Ma for carbonates (Sm-Nd), and 310 ± 5 Ma for brannerite were reported by Oberthür et al. (2009). The authors note several difficulties with the Re-Os method and prefer the more precise U–Pb age obtained from brannerite as representative of the age of ore mineralization.

The brannerite sample from California was described by Hewett et al. (1957) as occuring in a gray granite gneiss composed of quartz and potassium feldspar as major minerals, with minor amounts of plagioclase feldspar and biotite, and a suite of trace minerals including magnetite, zircon, monazite, xenotime, euxenite, and rutile. Brannerite occurs in this rock as nodules up to 5 × 5 cm in size. There is some uncertainty in the age of this locality, as the original description suggested that the gray gneiss might be Precambrian on the basis of textural features; however, they may be younger igneous rocks that have been deformed within a tectonic shear zone. Undeformed Mesozoic igneous rocks of similar mineralogy are also common in this region and euxenite from a granitic pegmatite in these igneous rocks gives an age of 150 Ma (Hewett et al., 1957). Furthermore, after making some corrections for biotite and rutile inclusions, the chemical analysis of brannerite reported by Hewett et al. (1957) gives a U–Th–Pb chemical age of ~220 Ma using Eqs. (1) and (2), therefore in the absence of more definitive data, we have assumed a rather broad Mesozoic age range of 65–250 Ma for the calculation of dose and dpa in this study.

Brannerite samples from Idaho, Switzerland, and France represent the youngest geological occurrences of brannerite included in this study. The sample from Idaho was found in a stream placer deposit at Kelly Gulch in the Stanley Basin area of Custer County and probably originated from the weathering of nearby Cretaceous granitic intrusions (Hess and Wells, 1920). We have assumed an age of 65–90 Ma for this sample based upon the known ages of muscovite-biotite type (Na rich) and hornblende-biotite type (K rich) intrusions in the area. In Switzerland, brannerite primarily occurs in relatively late stage, post-metamorphic granitic pegmatites in the Ticino region. These igneous rocks are generally intruded as dikes and consist of quartz, feldspars, and micas as the main minerals (Bianconi and Simonetti, 1967). Brannerite typically occurs as small single crystals or groups of crystals enclosed in quartz or K-feldspar together with minor amounts of rutile and scheelite. Other minerals in the pegmatites include molybdenite, arsenopyrite, apatite, and titanite. The granitic pegmatites of the Ticino region and have reasonably well established ages of 20–25 Ma (Graeser and Guggenheim, 1990). The French brannerite sample occurs in an Alpine hydrothermal quartz-barite vein at the La Gardette mine, near Bourg d' Oisans, Isere, where it occurs as individual bladed crystals or as groups of crystals enclosed within quartz and associated with gold, galena, sphalerite, and tetrahedrite (Geffroy, 1963). The most likely age range of Alpine veins in this region is on the order of 5–11 Ma based on a combination of Th-Pb and U-Pb dating of monazite and Ar-Ar dating of potassium feldspar (Gasquet et al., 2010).

4. SEM-EDX results

4.1. Microstructural observations

Brannerite samples with the oldest geological ages generally exhibit the most interesting microstructural features, including evidence for interaction with an aqueous fluid, formation of secondary alteration products, and the presence of cracks within the brannerite and in adjacent minerals. Samples from Crocker's Well (B1, B5, and B6) consist of variable amounts of unaltered and altered material. Sample B1 exhibits the most advanced level of geochemical alteration (Fig. 1A). A large proportion of this sample consists of altered brannerite, fine-grained clusters of TiO_2 (anatase?) typically 10–50 μm in size, and irregular patches of thorite. Another important result from the SEM work is the observation of fracturing of the associated rock matrix or inter-grown minerals, in this case, the associated primary rutile exhibits several microfractures that are filled with a poorly

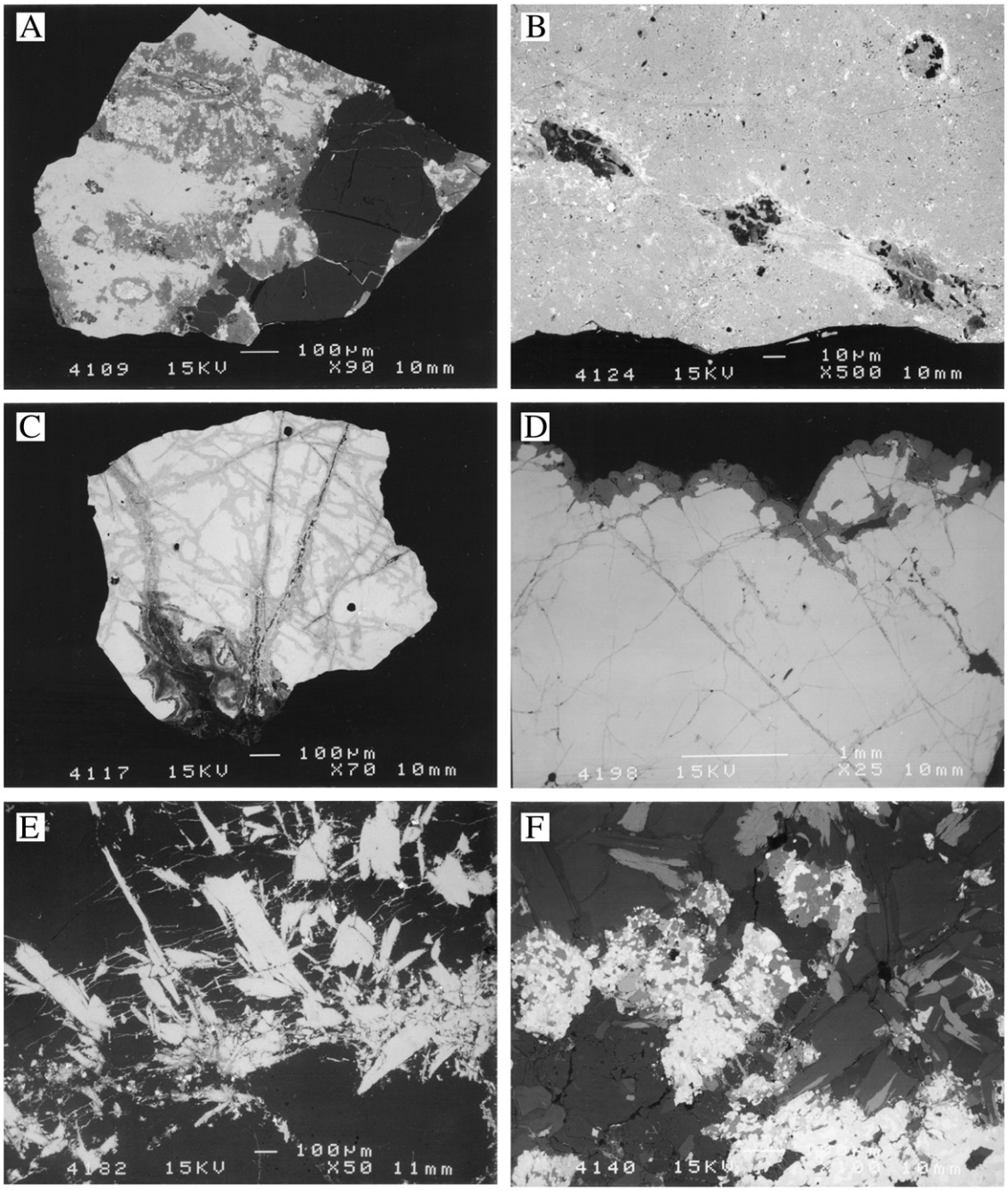

Fig. 1. Representative backscattered electron images of brannerite samples with geological ages greater than 100 Ma. A) Sample B1, Crocker's Well, South Australia, $t = 1580$ Ma, showing advanced effects of alteration (medium gray) and recrystallization to secondary phases, including thorite (white) and TiO_2 (small black patches, probably anatase). An area of primary rutile (dark gray) is present on the right hand side of the sample. Cracks present in the rutile may be due to volume expansion of the brannerite induced by alpha decay damage. Some of the cracks contain a poorly characterized secondary uranium oxide phase (light gray to white). B) Sample B4, Kansanshi mine, Western Province, Zambia, $t = 500$–520 Ma, showing relatively unaltered brannerite (light gray) with patches of altered material (medium and dark gray), TiO_2 (small black patches, probably anatase), and numerous patches and specks of uranium oxide and galena (white). C, D) Samples B2 and B10, Sierra Albarrana, Spain, $t = 350$–390 Ma, showing alteration confined to interior cracks and the outermost surface of the brannerite. The alteration exhibits darker gray contrast, but the gray level varies and becomes darker with increased Si content. E) Sample B8, Bou Azzer, Morocco, $t = 305$–315 Ma. This sample exhibits narrow zones of alteration (darker gray) around crystal rims and along interior cracks. Note that the host rock is cracked due to volume expansion of the brannerite, and these cracks are filled by secondary uranium oxide phases. F) Sample B7, San Bernardino County, California, $t < 250$ Ma. Brannerite in this sample is relatively unaltered and associated with a suite of rare element minerals (see text). The host rock primarily consists of biotite, albite, and quartz. Image magnification is exactly double that of the image shown in (E).

characterized U-oxide secondary phase. The other samples (not shown) from Crocker's Well are not as severely altered as sample B1, although they do contain patches and small spots of TiO_2, thorite, and galena. This result is generally consistent with observations made by Ludwig and Cooper (1984), who found that the color of brannerite changed from black at deeper levels to olive-brown nearer to the ground surface at Crocker's Well.

We examined one specimen from the Western Province, Zambia (B4), which exhibits a relatively uniform matrix of brannerite (Fig. 1B) with small patches of altered material (TiO_2 + unknown U-oxide) and numerous small particles of galena (generally < 5 µm in size). For the samples from Sierra Albarrana, Spain (B2, B10), alteration typically follows microfractures into the interior of the brannerite and in some cases there are variations in the backscattered

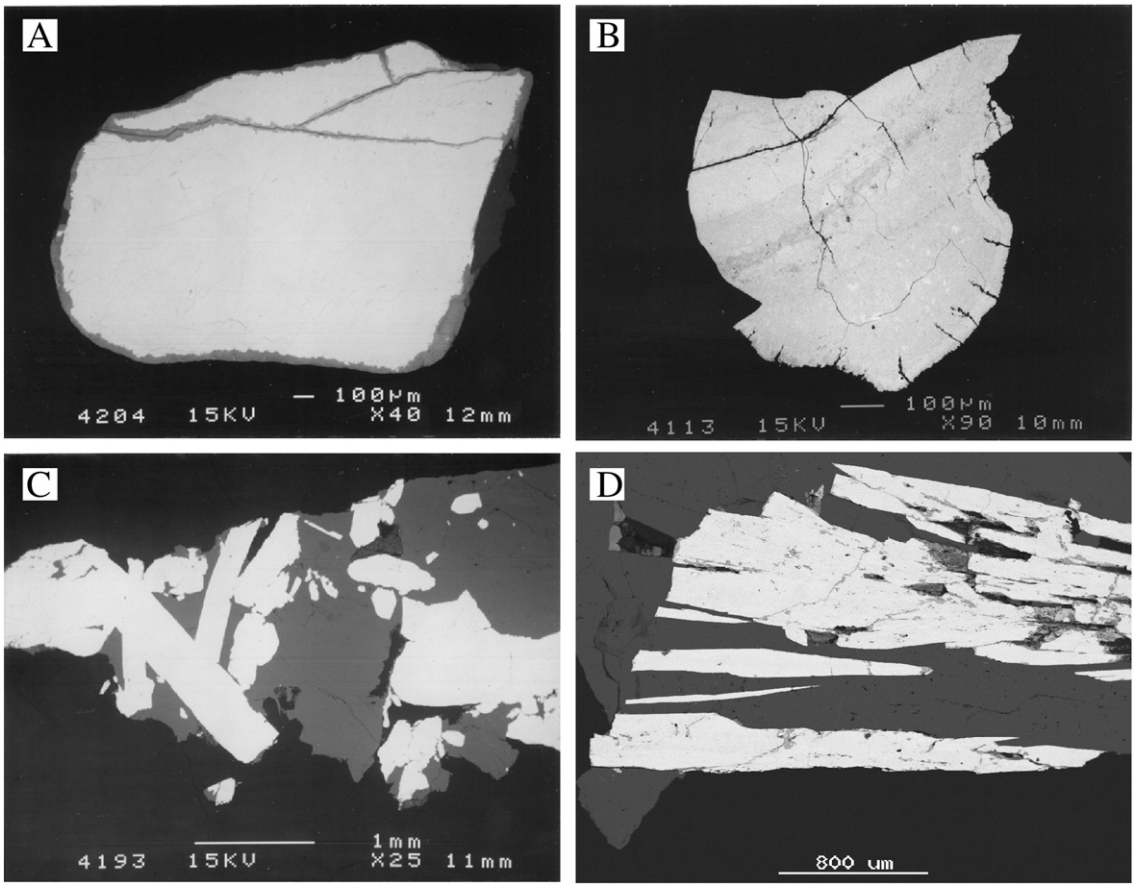

Fig. 2. Representative backscattered electron images of brannerite samples with geological ages less than 100 Ma. A) Sample 11, Stanley, Idaho, $t<80$ Ma. This sample was obtained from a placer deposit and shows alteration around the rim and along cracks in the interior of the grain. B, C) Samples B3 and B9, Ticino, Switzerland, $t=20$–25 Ma, showing alteration restricted to small cracks near the exterior of the grain in (B). This sample also shows possible primary compositional zoning. Sample B9 is relatively unaltered. D) Sample B13, Bourg d'Oisans, France, nominal $t=5$–11 Ma, appears to be unaltered, but exhibits minor alteration in localized areas along grain boundaries and small cracks.

electron contrast of the altered material, indicating that elemental concentration gradients may exist within the altered areas (Fig. 1C, D). SEM results for sample B8 from Bou-Azzer, Morocco also reveal the presence of alteration along grain boundaries and fractures (Fig. 2E). This specimen was found to contain patches of pyrite (with about 2 wt.% As), fine particles of galena and U-oxide, and a secondary TiO_2 phase, the latter being observed in the altered rims. In this sample, the quartz matrix is heavily fractured in the vicinity of the brannerite crystals and the fractures are filled with a poorly characterized U bearing material with considerable variation in backscattered electron contrast. Together with the above observations on sample B1, these results give a clear indication of local transport of U away from the source brannerite during alteration. A third example of fracturing of the rock matrix was observed in sample B12 from Switzerland (not shown), but in this sample the microfractures are largely barren, consistent with the low level of geochemical alteration in this specimen (see below).

The brannerite sample from California (B7) consists of relatively unaltered grains of brannerite (generally<50 µm) intimately associated with thorite, xenotime, zircon, allanite, rutile, and apatite (Fig. 1F). The matrix for this rare-element mineral assemblage consists of biotite, quartz, albite, and some chlorite that may be a retrograde alteration product of biotite. Although worth further detailed study, this specimen is very complex and warrants an independent investigation of the mineralogy and crystal chemistry. Any further study is therefore beyond the scope of this paper.

As noted above in Section 3, the sample from Stanley Idaho (B11) was obtained from a placer deposit; however, the SEM observations of this study show that the interior of the partly rounded grain shown in Fig. 2A appears to be relatively unaltered. In this specimen, alteration is confined to a region around the rim of the grain on the order of 100 µm in width and along a set of cracks running through the grain. Optical microscopy and SEM-EDX work revealed that the youngest samples of this study are either unaltered or exhibit only minor alteration. In particular, the samples from Switzerland (B3, B9, B12) and France (B13) appear to be either free of alteration or reveal evidence for alteration only at a high contrast setting of the BSE detector, suggesting that elemental changes between the unaltered and altered areas are minor. Alteration is usually confined within irregular patches, narrow veinlets, or around the rim of the sample (see Fig. 2B–D).

4.2. Chemistry of unaltered brannerite

Average compositions of relatively unaltered areas of each brannerite sample are given in Table 2 (assuming all Fe is Fe^{3+} and all U is U^{4+}). The range of compositions based on all of the analyses obtained in this study indicate that these natural brannerites contain 36–42 wt.% TiO_2, 30–57 wt.% UO_2, 0–15 wt.% ThO_2, 0–7 wt.% CaO, 0–7 wt.% PbO, 0–2 wt.% Nb_2O_5, 0–3 wt.% SiO_2, 0–2 wt.% Al_2O_3, 0–3 wt.% Fe_2O_3, 0–5 wt.% Y_2O_3, and 0–3 wt.% Ln_2O_3 (Ln = Ce, Nd, Sm, Gd). Both MnO and NiO were detected in various samples but it is unusual for these metal oxides to reach levels of 0.5–1.0 wt.% and Na_2O was not detected in any of the samples.

The chemical formula of brannerite was initially calculated from the SEM-EDX analyses by normalization to 6.00 oxygens. On this basis the cation total commonly exceeds the ideal value of 3.00 (range = 3.04–3.24) when normalized to 6.00 oxygen atoms,

Table 2
Average compositions of relatively unaltered areas of 13 brannerite samples.

	B1	B2	B3	B4	B5	B6	B7	B8	B9	B10	B11	B12	B13
Nb_2O_5	0.0	0.0	0.0	0.0	0.0	0.0	0.9	0.0	0.0	0.0	0.8	0.0	0.1
SiO_2	0.5	0.1	0.1	1.6	0.5	1.0	0.3	0.6	0.0	0.0	0.1	0.0	0.0
TiO_2	39.3	37.9	39.8	39.8	37.5	40.1	40.8	39.7	40.8	37.4	39.0	39.8	41.4
ThO_2	7.5	2.2	2.0	2.6	12.1	11.6	9.0	0.4	1.8	1.1	6.3	1.7	1.0
UO_2	40.2	50.0	55.3	45.1	36.6	36.7	38.4	50.6	55.9	52.0	46.5	56.5	52.8
Al_2O_3	0.2	0.9	0.2	0.8	0.3	0.2	0.3	0.2	0.1	0.3	0.2	0.0	0.2
Fe_2O_3	1.7	1.6	0.7	1.0	2.0	1.6	0.8	1.4	0.4	1.1	2.0	0.8	0.4
Y_2O_3	1.7	0.7	0.8	1.7	0.9	1.3	3.1	1.1	0.0	0.5	2.2	1.1	1.2
Ln_2O_3	2.2	0.3	0.4	1.2	1.3	1.5	1.5	1.1	0.2	0.4	1.1	0.0	1.7
CaO	1.5	3.5	0.5	3.2	4.5	2.3	3.4	2.8	0.5	4.1	1.4	0.0	0.3
MnO	0.1	0.3	0.0	0.1	0.1	0.1	0.1	0.5	0.0	0.1	0.0	0.0	0.1
NiO	0.0	0.0	0.0	0.0	0.0	0.6	0.0	0.5	0.0	0.0	0.0	0.0	0.0
PbO	5.3	2.5	0.2	3.0	3.2	3.2	1.5	1.1	0.2	3.2	0.6	0.2	0.2

indicating that a significant amount of the U must be in a higher valence state than the assumed U^{4+} state. Therefore, we re-normalized the analyses to 3.00 cations and calculated the amount of U^{6+} necessary to provide charge balance. Results of this exercise show that on average, all but one of the brannerite samples return $U^{4+}/(U^{4+}+U^{6+})$ ratios in the range of 0.35 to 0.95 (sample B5 returned an unusually low value of 0.14). There is some correlation between the calculated U valence state and geological age, with the following grouping of $U^{4+}/(U^{4+}+U^{6+})$ ratios: all of the Alpine samples (0.87–0.95), the Idaho brannerite (0.70), then all of the remaining older samples (0.14–0.53). The re-normalized analyses indicate that the A-site typically contains 0.45–0.88 U, and up to 0.31 Ca, 0.22 Th, 0.14 Y, and 0.07 Ln atoms per formula unit (*apfu*). Similarly, the B-site typically contains 1.74–2.10 Ti, and up to 0.15 Fe, 0.14 Si, 0.09 Al, 0.06 Nb, 0.04 Mn, and 0.04 Ni *apfu*. With few exceptions, the cation totals for the A-site and B-site are mostly within the ranges 0.90–1.05 and 1.95–2.10 *apfu*, respectively, suggesting that there may be minor deviations from AB_2O_6 stoichiometry in these heavily radiation damaged samples.

Analyses of the nominally unaltered brannerite samples are summarized in Fig. 3, where we have plotted the most significant correlations together with other data having a possible bearing on post-crystallization chemical effects and interactions with late stage fluids. For the B-site, a good negative correlation was observed for Ti and Fe + Al, with slope = −0.53 and correlation coefficient R = 0.78 (Fig. 3A). Including other B-site cations (Nb, Mn, and Ni) with Fe + Al changes the slope of the fit slightly but does not significantly improve the correlation. The amount of Si incorporated in nominally unaltered brannerite is quite high, up to 0.15 apfu, but the correlation with Ti is not very good (Fig. 3B), and extensive occupancy of octahedral sites by Si is not normally expected in oxide compounds at low pressure. With regard to the A-site cations, we observe a very good negative correlation between U and Th, with slope = −0.45 and R = 0.86 (Fig. 3C). Although Ca is the second most abundant A-site cation in brannerite, the correlations with Th and U are weakly positive and negative, respectively (Fig. 3D, E), a result that is difficult to rationalize without invoking coupled substitutions with B-site cations or oxygen and hydroxyl groups. The variable valence state of U is also an issue in these samples, but because it has not been determined experimentally, the real statistical variation of U^{4+}, U^{5+}, and U^{6+} against other elements cannot be evaluated. Nevertheless, there is a very good negative correlation between U and the summation of Ca, Y, Ln, and Th with slope = −1.2 and R = 0.84 (Fig. 3F).

4.3. Geochemical alteration

Average compositions of altered areas of the brannerite samples determined by SEM-EDX are given in Table 3. The results indicate that the altered areas show a considerable range of chemical modification, with ranges of 38–77 TiO_2 and 3.3–43.6 UO_2 (in wt.%) for the essential brannerite components together with maximum amounts of 12.3 Fe_2O_3, 3.0 Al_2O_3, 1.5 Nb_2O_5, and 0.2 MnO for the nominal group of B-site components and up to 13.5 ThO_2, 10.2 PbO, 4.3 CaO, 2.3 Ln_2O_3, and 1.6 Y_2O_3 for the nominal A-site components. Geochemical alteration of brannerite also leads to increases in the atypical components SiO_2, As_2O_5, and P_2O_5 with these oxides reaching maximum values of 16.5, 5.9, and 4.3 wt.%, respectively. As in the unaltered brannerite, Na_2O is also consistently near or below the detection limit of approximately 0.1 wt.% in the altered areas. Comparison of Tables 2 and 3 suggest that, on average, the brannerite samples investigated in this study have lost between about 8 and 93% of the U as a result of geochemical alteration processes. These results are summarized in Fig. 4, where we plot the Si/Ti ratio versus U/Ti for all analyses obtained in this study. Here we can see that the data for nominally unaltered brannerite cluster between U/Ti = 0.23–0.43 with maximum Si/Ti ratios of about 0.08. Although the data points for the altered brannerite appear to fall into three groups, possibly due to inadequate sampling, the overall trends are generally consistent with simple U loss or U loss coupled with uptake of Si from the associated aqueous fluid phase.

The analytical data from unaltered and altered areas of the brannerite samples were also used to calculate a set of distribution coefficients, K_d, after normalization of the cation proportions to Ti. In this study, we set $K_d = K_{a/u}$, where $K_{a/u}$ is the atomic composition of the altered area divided by the atomic composition of the unaltered area of the sample. This distribution coefficient serves as the geochemical exchange parameter or enrichment/depletion factor for element mobility during alteration. The results are summarized in Table 4. Because P and As were not detected in any of the nominally unaltered brannerite samples, the reported $K_{a/u}$ results for these elements are all minimum values. However, the data show that P is consistently enriched in altered brannerite, in some cases by at least a factor of 30 relative to unaltered areas of the same sample. It is noteworthy that As in enriched in by a factor of at least 105 in the high Si areas of sample B8 from Bou-Azzer, Morocco. Although the behavior of Si was presented above in some detail (see Fig. 4), the enrichment factors listed in Table 4 provide a more quantitative description of the variation within and between samples. We find that $K_{a/u}$ for Si is greater than 10 in more than half of the average analyses reported in this work and reaches a value greater than 60 in sample B10 from Sierra Albarrana, Spain. With regard to the actinides, Th proves to be relatively immobile in most of the brannerite samples with a significant depletion by a factor of 2.5 in the Si poor alteration zone of sample B3 and enrichment by a factor of 4.6 in the Si rich altered area of sample B8. This result is interesting in view of the evidence of U loss presented above (Fig. 4), e.g., the distribution coefficients listed in Table 4 show that U is depleted in the altered brannerite by a factor of 2–10 in most of cases reported here.

For the other elements of interest, Al either remains immobile or is enriched typically by a factor of 2–3 in the altered brannerite areas, with $K_{a/u}$ values above 5 observed in three cases. Apart from minor

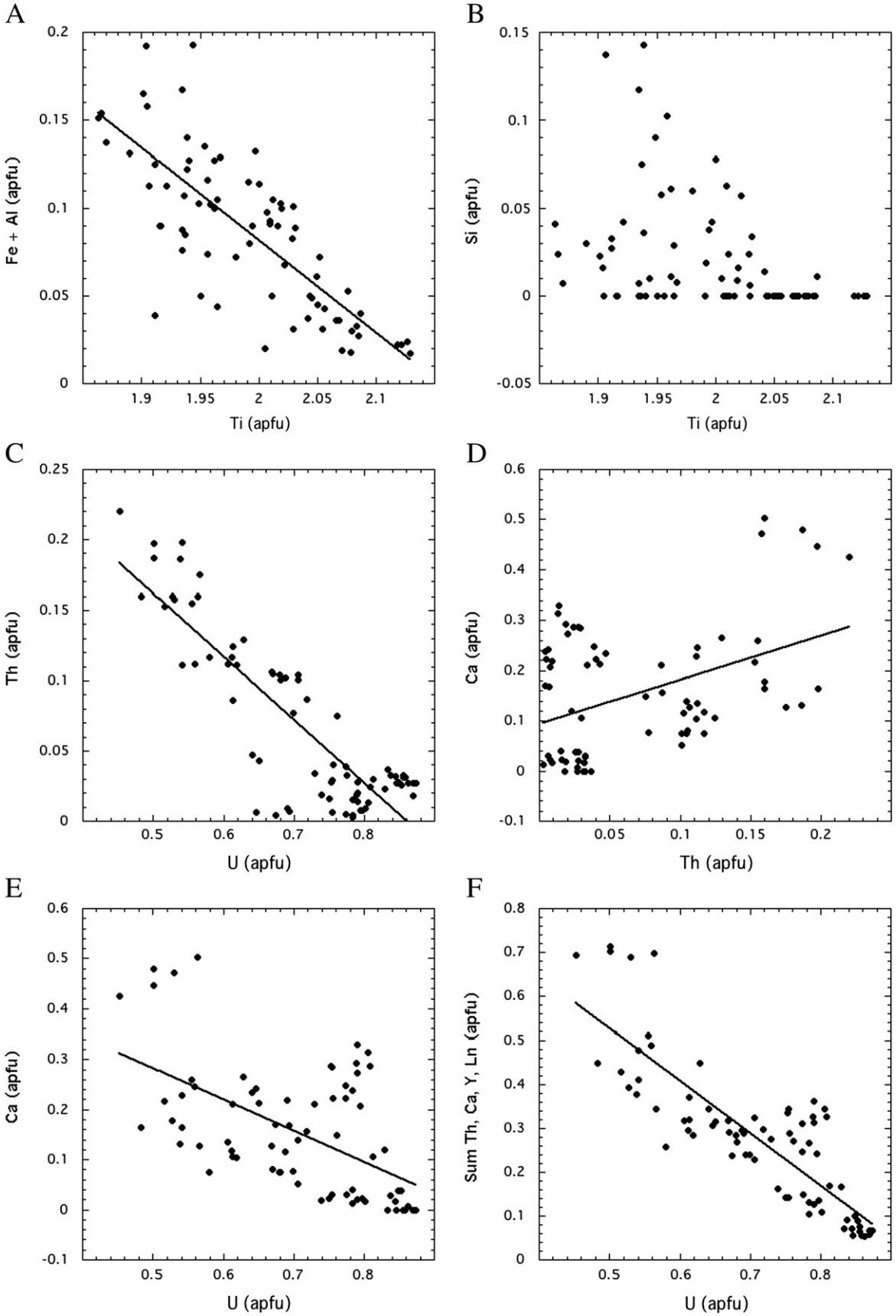

Fig. 3. Plots of the chemical composition of relatively unaltered brannerite in atoms per formula unit. A) Negative correlation between Ti and Fe + Al; this is the only major trend observed for B-site cations and implies that a coupled substitution must exist in order to account for charge balance. B) Relatively unaltered brannerite contains significant amounts of Si but the correlation with Ti is poor. C) A good negative correlation is observed between U and Th, consistent with the simple substitution of Th^{4+} for U^{4+} controlled by the host rock geochemistry. D, E) the behavior of Ca is more complicated and it shows a weak positive correlation with Th and a negative correlation with U, respectively. F) As expected, there is a good negative correlation between U and the sum of Th, Ca, Y, and Ln cations on the A-site.

Table 3
Average compositions of altered areas of brannerite samples.

	B1	B3a	B3b	B6	B8a	B8b	B10a	B10b	B11a	B11b	B13
P_2O_5	1.1	1.5	1.5	0.1	0.0	0.1	4.3	0.4	3.3	0.4	0.1
As_2O_5	0.0	0.0	0.0	0.2	1.9	5.9	0.0	0.0	0.0	0.0	0.1
Nb_2O_5	0.0	0.0	0.0	0.1	0.2	0.2	0.0	0.0	1.5	0.8	0.3
SiO_2	16.5	6.2	1.0	11.6	1.8	9.6	0.4	3.6	3.8	1.6	2.6
TiO_2	45.5	47.3	76.7	47.6	69.5	38.9	73.6	39.4	62.8	42.3	57.2
ThO_2	13.5	3.0	1.8	13.1	1.1	1.8	3.0	1.0	8.9	5.8	1.0
UO_2	8.2	27.9	9.4	11.3	17.0	32.1	7.5	43.6	3.3	42.5	23.7
Al_2O_3	0.6	1.1	1.7	0.6	1.0	0.4	3.0	1.0	2.0	0.0	0.3
Fe_2O_3	1.8	1.3	4.2	1.4	4.4	0.6	3.9	1.1	12.2	1.3	4.8
Y_2O_3	0.1	0.1	0.0	0.4	0.0	0.1	0.0	1.2	0.0	1.6	0.5
Ln_2O_3	1.5	0.7	0.0	2.2	0.1	0.6	0.2	2.1	0.2	1.3	2.3
CaO	3.6	0.6	0.3	4.3	0.9	3.3	1.1	2.1	0.7	0.6	1.0
MnO	0.0	0.1	0.0	0.1	0.0	0.0	0.1	0.2	0.0	0.1	0.1
NiO	0.0	0.0	0.0	0.0	0.0	0.0	0.0	0.0	0.0	0.0	0.0
PbO	7.6	10.2	3.4	7.0	2.1	6.4	2.9	4.3	1.3	1.7	6.0

variation, Fe appears to be relatively immobile in most of the samples. It is depleted by a factor of 2.5 in the Si rich part of sample B8, shows variable behavior in the altered areas of B11, and is enriched by a factor of 8.7 in the altered areas of B13. Except for one sample (B10), Y is consistently depleted in the altered brannerite, in many cases by a factor of 10 or more. This pattern is not followed by the lanthanides, which exhibit depletion by a factor of up to 10 in half of the cases examined and enrichment by a factor of up to 4.7 in the other cases. A similar behavior is found for Ca, although not necessarily in the same samples, and in most cases Pb tends to be enriched by a small amount in the altered brannerite. In sample B13 from France, Pb shows an unusually large enrichment factor of 21.7, possibly due to enrichment of common Pb this Alpine vein system (in the form of galena precipitates in the altered areas?).

5. TEM results

Electron diffraction patterns were obtained from relatively unaltered areas of all of the brannerite samples examined in this study.

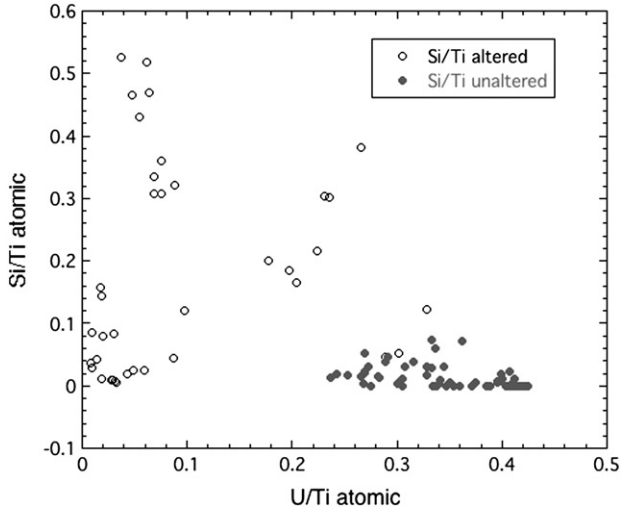

Fig. 4. Graphical representation of the behavior of Si in unaltered (gray circles) altered brannerite (open circles). Here, the variation is expressed as the U/Ti atomic ratio versus the Si/Ti atomic ratio because alteration leads to signification deviation from AB_2O_6 stoichiometry. This plot shows the significant variation of U content and small amounts of Si incorporated in nominally unaltered brannerite. Altered samples may exhibit considerable loss of U; however, the Si content shows broad variation with U loss. See text for discussion and additional information regarding the linear fits.

In regions where the samples appear to have no inclusions or where the abundance of the inclusions is low, the SAED patterns typically consist of two broad, diffuse rings characteristic of amorphous materials. In each case, the diffuse rings have equivalent d-spacings of 0.31 Å and 0.19 nm, similar to those of many other metamict oxide minerals (Headley et al., 1981; Ewing and Headley, 1983; Lumpkin and Ewing, 1988; Lumpkin, 1992; Lumpkin et al., 1994a). Representative SAED patterns, intensity profiles, and bright field images of fully amorphous areas of samples B1, B3, B10, and B4 are shown in Figs. 5–7. Bright field images of these grains are typically featureless, consistent with the absence of long-range periodicity in the material following prolonged alpha decay damage to doses in excess of 10^{16} α mg^{-1}.

Many of the samples examined thus far also exhibit weak diffraction spots in SAED patterns taken from areas having a sufficient number of inclusions. In most cases, the diffraction spots appear to be due to the presence of 5–100 nm crystallites of a U-oxide phase (Figs. 6B and 7A). Measurement of the limited number of diffracted beams in the SAED patterns in samples B10 and B4 indicate that the inclusions may be uraninite, with d-spacings of 0.32, 0.27, and 0.16 nm. This was confirmed by qualitative EDX analyses of several of the larger inclusions found near the thin edges of several brannerite grains. Some of the grains in sample B4 from the Western Province of Zambia were also found to contain 10–200 nm sized spherical voids (Fig. 7B), similar to previous observations on metamict zirconolite and columbite (Ewing and Headley, 1983; Lumpkin, 1992). These voids have been attributed to the accumulation of radiogenic He in the sample over time.

Although a detailed analysis of altered brannerite at the TEM scale is beyond the scope of this work, we present a limited set of results for sample B13, primarily to address the issue of the nature of the secondary TiO_2 phase. Diffraction patterns and bright field images (Fig. 8) of the altered brannerite in this sample demonstrate that it consists of a mixture of both crystalline and amorphous material as shown by the presence of diffraction spots and diffuse rings, respectively. Measurement of d-spacings from the crystalline component is consistent with the presence of brookite with some anatase and a possible contribution from galena. TEM bright field images of this sample indicate that the crystallite dimensions are on the order of 50 nm or less.

6. Discussion

6.1. Implications of U–Th–Pb chemical ages

Of most interest here are the samples from Crocker's Well, South Australia (B1, B5, and B6). In Fig. 9 we show a time-temperature plot that illustrates some aspects of the geological history of the Olary region (data from Ludwig and Cooper, 1984; Clarke et al., 1986; Foden et al., 2006) together with the available chemical and isotopic U–Th–Pb ages. The data point at 1580 Ma is the U–Th–Pb isotopic age and minimum closure temperature of zircons from granitic rocks associated with the brannerite deposit at Crocker's well. The data points at 1466 and 490 Ma represent the closing phases of Olarian and Delamerian metamorphism, respectively. We have also included a data point at 770 Ma in an effort to approximate the temperature during the Neoproterozoic (542–1000 Ma). This estimate is based on the approximate thickness of overlying sediments (Paul et al., 2000) in the vicinity of Crocker's Well, assuming a geothermal gradient of 30 °C km^{-1}. The remaining data points at 446 and 301 Ma represent the ages closure temperatures obtained from Rb–Sr dating of biotite and fission track dating of apatite, respectively. All of these data define the time-temperature history (Fig. 9); however, this trend is poorly constrained between the two metamorphic episodes due to lack of specific data relevant to the cooling and exhumation of the Olary terrain.

Table 4
Enrichment-depletion factors of altered brannerite samples based on Ti-normalized, atomic compositions. These factors are calculated relative the unaltered composition.

	B1	B3a	B3b	B6	B8a	B8b	B10a	B10b	B11a	B11b	B12	B13
P	>13.6	>17.9	>11.0	>1.2	–	>1.5	>32.9	>5.7	>29.6	>5.3	>2.8	>1.0
As	–	–	–	>2.9	>19.0	>105.5	–	–	–	–	–	>1.2
Si	28.4	49.7	4.9	9.8	1.7	16.3	>3.6	>60.8	23.5	14.7	–	>30.2
Th	1.6	1.1	0.4	1.0	1.6	4.6	1.4	0.9	0.9	0.9	0.9	0.7
U	0.2	0.5	0.1	0.3	0.2	0.7	0.1	0.8	0.1	0.8	1.0	0.3
Al	2.6	1.0	0.9	2.5	2.9	2.0	5.1	3.2	6.2	<0.3	>7.8	1.1
Fe	0.9	0.7	1.3	0.7	1.8	0.4	1.8	1.0	3.8	0.6	0.9	8.7
Y	0.1	0.1	<0.1	0.3	<.1	0.1	<0.1	2.3	<0.1	0.7	0.6	0.3
Ln	0.6	1.8	<0.3	1.2	0.1	0.5	0.2	4.7	0.1	1.0	>3.5	2.6
Ca	2.1	0.1	0.1	1.6	0.2	1.2	0.1	0.5	0.3	0.4	1.8	2.4
Pb	1.2	3.3	0.7	1.8	1.1	5.9	0.5	1.3	1.3	2.6	1.0	21.7

Although imprecise, our average U–Th–Pb chemical ages of 350–680 Ma (Table 1) for unaltered brannerite are consistent with episodic loss of Pb due to Delamerian metamorphism at 490–514 Ma. This conclusion is supported by the U–Th–Pb isotopic ages of 550–670 Ma determined on two brannerite samples by Ludwig and Cooper (1984) and previous U–Pb analyses that returned age dates of 515–665 Ma (Campana, 1954; Greenhalgh and Jefferey, 1959). Based on the microanalytical and microstructural data presented in this study, it is possible to understand the results of age dating of bulk samples of brannerite from the partitioning of parent and daughter products between unaltered material, altered areas, and any U–Th–Pb secondary phases present:

$$U_{tot} = x_{unalt}U_{unalt} + x_{alt}U_{alt} + \Sigma_i x_{sec}U_{sec} \quad (5)$$

$$Th_{tot} = x_{unalt}Th_{unalt} + x_{alt}Th_{alt} + \Sigma_i x_{sec}Th_{sec} \quad (6)$$

$$Pb_{tot} = x_{unalt}Pb_{unalt} + x_{alt}Pb_{alt} + \Sigma_i x_{sec}Pb_{sec}. \quad (7)$$

These equations give the total amounts of U, Th, and Pb present depending on the phase proportions (x_i) and distribution of U, Th, and radiogenic Pb between the unaltered brannerite, the altered material, and any secondary U–Th–Pb phases formed within the sample. Open system behavior is clearly defined using this approach, in the case of the samples from Crocker's Well the U–Th–Pb ages are mainly affected by U loss from the altered material and Pb loss from both unaltered and altered areas, although a higher proportion of Pb is lost from the unaltered material (Tables 2 and 3). Thus, older ages are expected in bulk samples with a higher proportion of altered material due to extensive

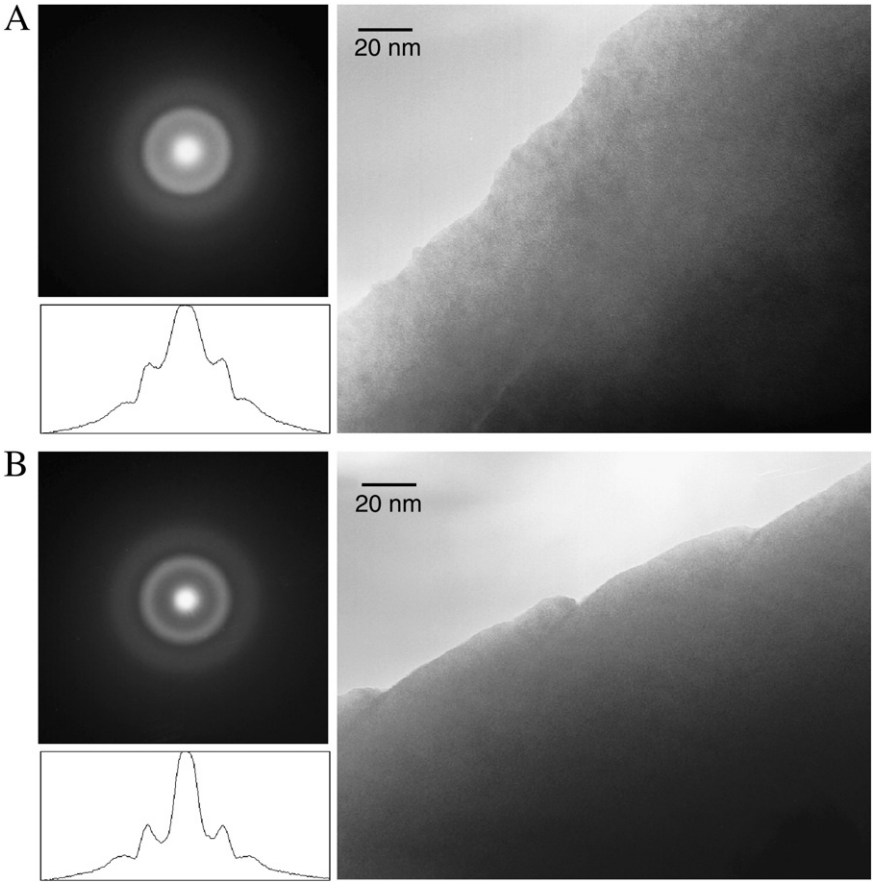

Fig. 5. Representative selected area electron diffraction (SAED) patterns, intensity profiles, and TEM bright field (BF) images of relatively unaltered natural brannerite samples. A) Sample B1, Crocker's Well, South Australia. B) Sample B3, Ticino, Switzerland. These results are typical for fully amorphous brannerite, with the SAED patterns showing prominent diffuse rings and no Bragg beams from crystalline material, while the corresponding BF images are relatively featureless.

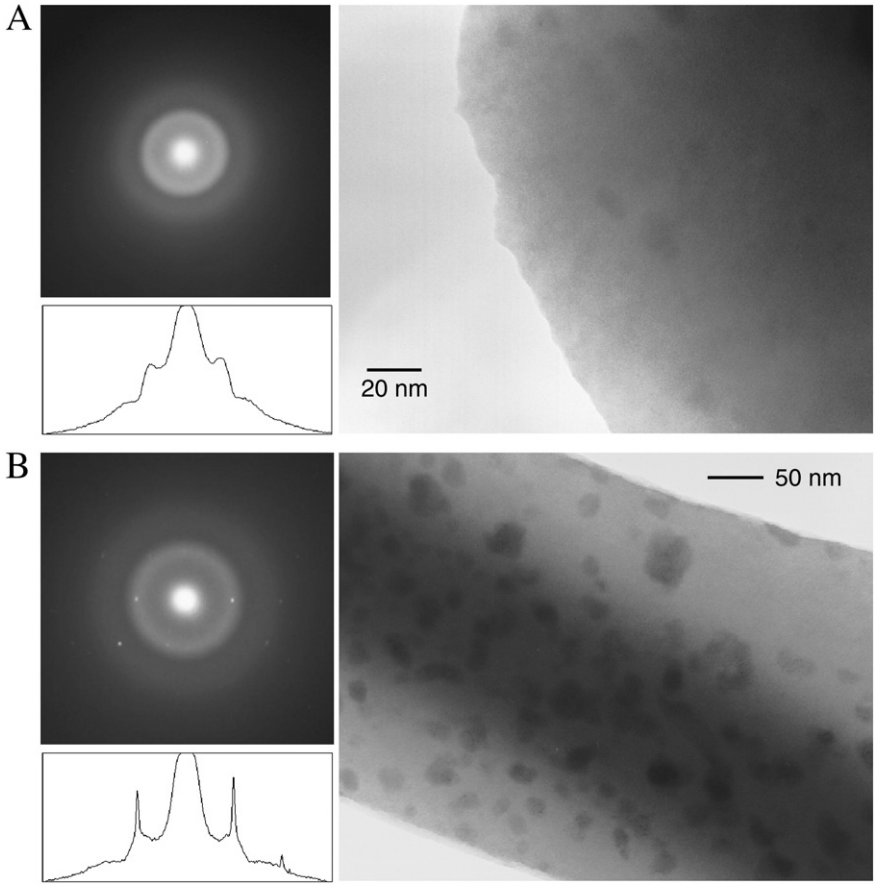

Fig. 6. Representative SAED patterns, intensity profiles, and BF images of relatively unaltered natural brannerite samples. A, B) Samples B2 and B10, respectively, Sierra Albarrana, Spain. These sets of SAED patterns and BF images show how the abundance of UO_2 inclusions varies from sample to sample; it may also vary considerably within the same sample.

loss of U from these areas combined with greater retention of radiogenic Pb. The ability of Pb to serve as a network modifier within the Ti–Si–O framework of the glass-like structure of altered brannerite provides a reasonable explanation for the preferential retention of radiogenic Pb in the altered phase (Table 4). Laboratory annealing studies of sample B10 (Zhang et al., 2006) demonstrate that amorphous brannerite begins to recrystallize between 500 and 700 °C and, as expected from crystal chemical considerations, this is accompanied by Pb loss from the brannerite. At higher annealing temperatures, the presence of Si and Al in this sample led to the formation of an alumino-silicate glass phase that retained both Ca and Pb.

For the brannerite sample from the Western Province, Zambia, the age of 465 Ma determined by SEM-EDX microanalysis in this study is consistent with Pb loss on the order of 7–10% based on the known age range (Table 1); however, the radiogenic Pb lost from the radiation damaged brannerite may be largely trapped within particles of galena observed in the specimen. This observation is consistent with previous studies of radiation damaged zirconolite and pyrochlore group minerals that have been exposed to fluids containing S species (Lumpkin et al., 1994b; Lumpkin and Ewing, 1995, 1996). For the two samples from Sierra Albarrana, Spain, one sample returned an age within the estimated age range; whereas, the other sample returned an older age. The reason for this discrepancy is unclear; however, it is possible that the brannerites are older than the nominal age range and represent different degrees of Pb loss as a direct result of Variscan metamorphism. This is consistent with the occurrence of the host pegmatites in rocks of lower Paleozoic age and the fact that the age range cited in Table 1 is based on $^{40}Ar/^{39}Ar$ dating of amphibole and muscovite, both of which can be interpreted as cooling ages, e.g., after the peak of metamorphism in this region (Azor and Ballèvre, 1997). In the case of the sample from Bou Azzer, Morocco, we determined an average age of 191 Ma based on microanalyses of the unaltered brannerite, considerably younger than the "bulk" U–Pb age of 310 Ma (Oberthür et al., 2009). This result is consistent with loss of 37–40% of the radiogenic Pb from the unaltered areas of the sample; however, this sample also contains abundant fine particles of galena, providing evidence for local trapping of Pb in a metal-sulphide hydrothermal system.

The Mesozoic brannerite samples from granitic rocks of San Bernardino County, California and Stanley Gulch, Custer County, Idaho give chemical U–Pb ages that are in reasonable agreement with the estimated host rock ages and U–Th mineral ages. In the case of the San Bernardino brannerite, the average age of 178 Ma indicates formation in the mid-Jurassic, consistent with the limited geological background data summarized earlier. Our average U–Th–Pb chemical age of 72 Ma for the sample from Idaho is remarkably consistent with the nominal age of the late Cretaceous granitic rocks in the Stanley Gulch area. Nevertheless, this age determination could be somewhat low as the altered areas of the sample, although volumetrically small, contain significantly higher Pb concentrations (Tables 2–4). All of the younger brannerite samples from Swiss Alpine pegmatites give upper limit chemical U–Th–Pb ages that are consistent with the established ages of the host rocks. The nominal age of the brannerite sample from Bourg d'Oisans, France is considerably younger than the upper limit U–Th–Pb age (Table 1), due to the detection limit constraints imposed by the SEM-EDX analytical technique.

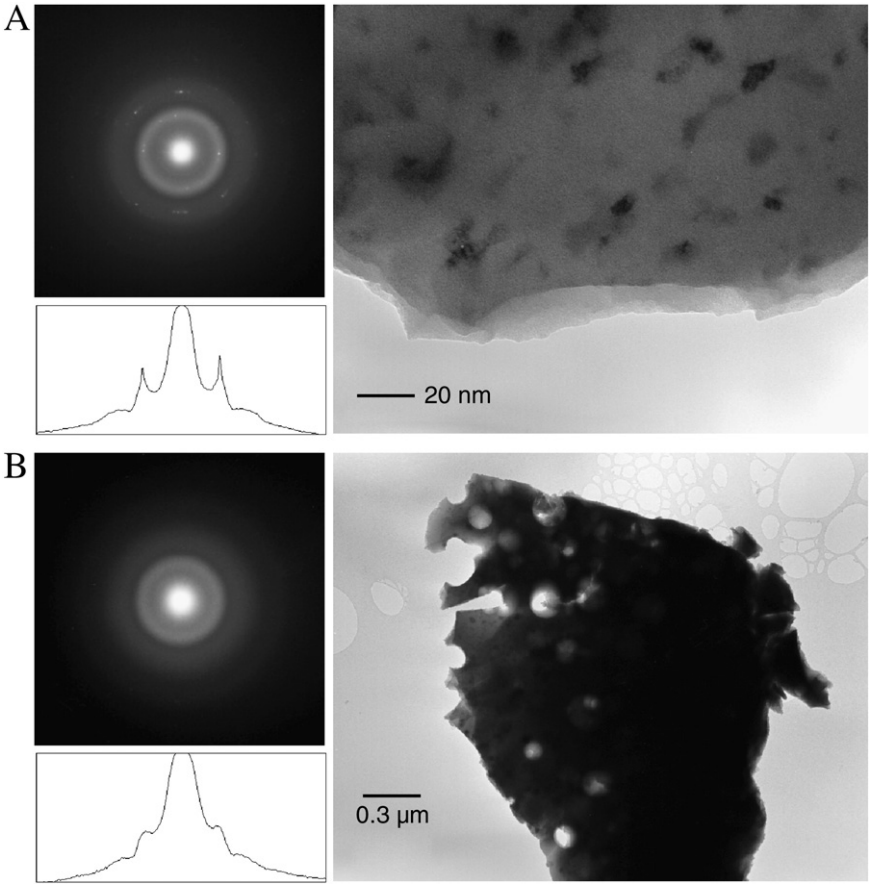

Fig. 7. Representative SAED patterns, intensity profiles, and BF images of relatively unaltered natural brannerite samples. A, B) Both sets of images are from samples B4, Kansanshi Mine, Western Province, Zambia. The SAED pattern and BF image in A) reveals the presence of UO_2 and other inclusions and B) shows the presence of sub-spherical voids, possibly related to the accumulation of radiogenic He in the sample over time.

6.2. Crystal chemistry of natural brannerite

The compositions of relatively unaltered areas of brannerite determined in this work are generally consistent with older chemical analyses reported in the literature (e.g., Hess and Wells, 1920; Pabst, 1954; Hewett et al., 1957; Campana and King, 1958; Bianconi and Simonetti, 1967). Our results demonstrate that the U content of natural brannerite is quite variable and that U can be replaced by significant amounts of Ca, Th, Y, and lanthanides, up to about 50–60% of the A-site in total. For the A-site cations, the substitution $Th^{4+} \rightarrow U^{4+}$ is straightforward; however, more complicated coupled substitutions must be postulated for Ca, Y, and Ln substitution. The most likely substitutions on the A-site are $Ca^{2+} + U^{6+} \rightarrow 2U^{4+}$ and $(Y, Ln)^{3+} + U^{5+} \rightarrow 2U^{4+}$. We also found that the Ti content is less variable than U in natural brannerite, with minor replacement of Ti by Fe, Si, Al, Nb, Mn, and Ni up to a maximum of around 20% of the B-site occupancy. The incorporation of trivalent transition metals can only be partly explained by the coupled substitution $(Fe, Al)^{3+} + Nb^{5+} \rightarrow 2Ti^{4+}$ up to a maximum of 0.06 Nb *apfu*, this is also the charge compensation mechanism in coexisting primary rutile. In this case, it is possible that some the deficient charge on the B-site is also compensated by U^{5+} or U^{6+} on the A-site, but this is difficult to confirm.

Another possible charge compensation mechanism for Fe^{3+} or any other B-site cations with valence states less than four in natural brannerite is substitution of OH^- for O^{2-}, but this remains open to question pending detailed investigation by quantitative microanalysis, thermal analysis, and infrared spectroscopy. The available chemical analyses in literature cited above indicate that natural, radiation damaged brannerite typically contains <0.1 to 3.7 wt.% H_2O, with one analysis of material from Crocker's Well giving an H_2O+ (released above 105 °C) value of 7.4 wt.%. Although the partitioning of this water between OH^- and H_2O is unknown, it's presence does support the possibility of charge compensation by OH^- groups.

The role of Si in unaltered brannerite is unclear, although we nominally include it on the B-site, the data shown in Fig. 3B show that there is a poor correlation between Si and Ti. Since the SEM and TEM results of this study have failed to provide evidence for micro-scale or nano-scale inclusions of a discrete silicate phase, we believe that the Si is located somewhere within the brannerite structure. In principle, Si is unlikely to substitute for Ti in octahedral coordination above trace levels at low pressure and may instead occupy interstitial sites in the structure. This issue remains to be resolved through the application of careful synthesis and characterization methods and a more detailed quantitative electron probe microanalysis study.

Calculated formulae based on 6 oxygen atoms suggest that some of the U may be present in a higher valence state. These results are generally consistent with the older chemical analyses wherein both UO_2 and UO_3 are reported, giving $U^{4+}/(U^{4+} + U^{6+})$ values between 0.0 and 0.9 (see Pabst, 1954; Hewett et al., 1957; Campana and King, 1958; Bianconi and Simonetti, 1967). Where direct comparisons can be made, we find that the literature data for one Alpine sample gives $U^{4+}/(U^{4+} + U^{6+}) = 0.9$, consistent with the range observed in this study. In three other instances, chemical analyses of samples from Crocker's Well and San Bernardino County, California, both have $U^{4+}/(U^{4+} + U^{6+})$ values of ~0.0 and a sample from Idaho gives $U^{4+}/(U^{4+} + U^{6+}) = 0.24$. All of these analyses give higher U valence states than the estimates presented here by SEM-EDX microanalysis. One issue with these older analyses is that they may

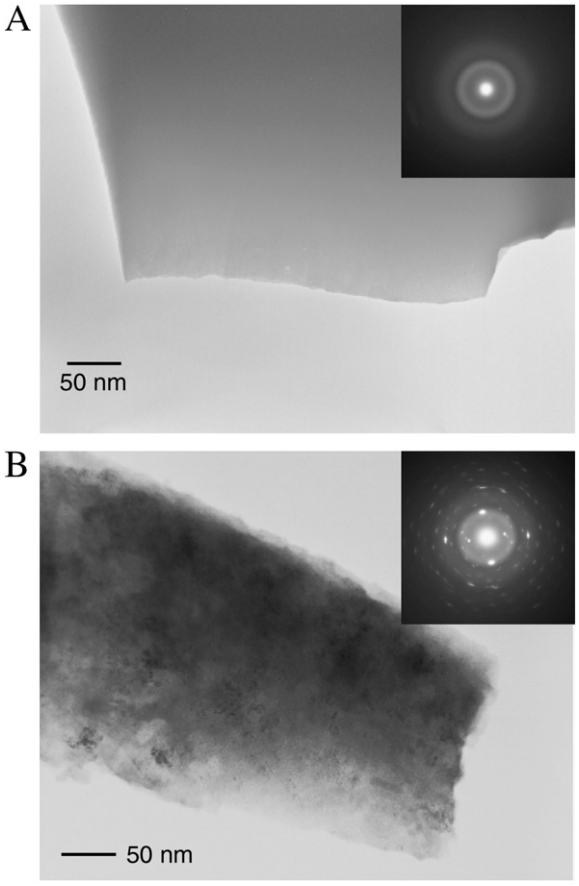

Fig. 8. Representative SAED patterns and BF images of unaltered and altered material in sample B13, Bourg d'Oisans, France. A) Unaltered amorphous brannerite. B) Altered brannerite showing a mixture of amorphous and crystalline material (brookite is the main secondary phase).

contain surface material or altered material with U in higher valence states included in the bulk analysis procedure. Direct measurements on unaltered areas of two of our samples by electron energy loss spectroscopy (Colella et al., 2005), on the other hand, give somewhat lower $U^{4+}/(U^{4+}+U^{6+})$ atios of 0.65 for a sample from the Swiss Alps and 0.60 for a sample from Spain. Recent synthesis work which shows that up to 0.3 atoms per formula unit of Ca or Gd can be substituted for U in brannerites heated in air or argon at 1350–1450 °C. Diffuse reflectance spectroscopy and X-ray photoelectron spectroscopy measurements conducted on these synthetic samples indicates that some U is present as U^{5+}, thereby providing a charge-balancing mechanism for incorporation of Ca and Gd (Vance et al., 2001; Finnie et al., 2003).

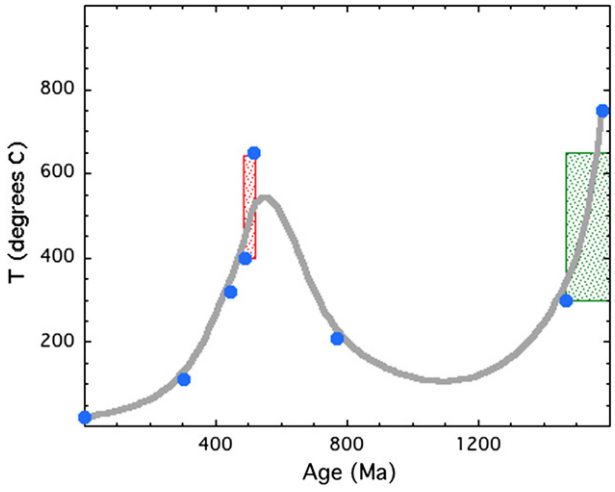

Fig. 9. Geological history and U–Th–Pb age dating results for brannerite samples from Crocker's Well, South Australia. A) Estimation of the time-temperature history, derived from geological data and closure temperatures for fission tracks in apatite, the Rb–Sr isotopic system in biotite, and the U–Th–Pb isotopic systems in zircon.

6.3. Brannerite stability in natural systems

The results of this study demonstrate that natural brannerite is susceptible to geochemical alteration in natural environments, with substantial loss of U from altered areas and loss of Pb from unaltered areas and to a lesser extent, altered areas. The observed U loss is partly compensated by incorporation of large amounts of Si and other elements from the attending fluid phase, including Al, P, and As, the latter being restricted to hydrothermal metal-sulphide ore deposits such as Kansanshi, Western Province, Zambia and Bou Azzer, Morocco. During alteration, Y is also typically removed from the altered brannerite, but the behavior of Fe, Ca, and Ln are more erratic and these elements may be either lost or gained. The range of compositions observed is entirely consistent with the variation in gray levels seen in the BSE images of altered brannerite. Furthermore, the quantitative evidence for U loss is consistent with the observation of U rich material located within fractures extending into the host rock matrix in two of the natural brannerite samples.

Although we have ample evidence for the chemical alteration of brannerite, there is very little direct evidence for corrosion or total dissolution of the brannerite matrix (Ifill et al., 1966; Szymanski and Scott, 1982). The samples available for this investigation generally do not show extensive replacement features or other physical indicators of corrosion. However, the observed alteration patterns are indicative of a dissolution-reprecipitation mechanism with variable uptake of Si from the associated aqueous fluid phase and release of U as transportable, uranyl complexes. Under relatively acidic conditions with the uranyl ion as the major stable carrier of U, the following equations provide a

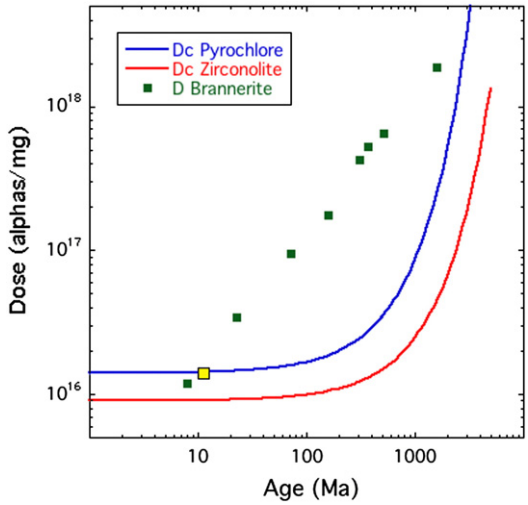

Fig. 10. Plot of geological age versus dose for unaltered brannerite samples of this study (green squares). Included for reference are the critical dose curves for natural pyrochlore (blue) and zirconolite (red) derived from studies numerous suites of samples from different localities, with different ages and U-Th contents. All samples examined in this study have been rendered amorphous by alpha decay damage and therefore no critical dose can be obtained. Included for reference is the partly crystalline sample from Binntal Switzerland (Graeser and Guggenheim, 1990), shown as a yellow square symbol. These data suggest that the critical dose for amorphization of natural brannerite is close to that of natural pyrochlore for $t \sim 10$ Ma. See text for further discussion and implications.

general description of the alteration of natural brannerite (see Fig. 4):

$$2H^+ + 0.5O_2 + UTi_2O_6 = 2TiO_2 + [UO_2]^{2+} + H_2O \quad (8)$$

$$2H^+ + 0.5O_2 + [SiO_2] + UTi_2O_6 = SiTi_2O_6 + [UO_2]^{2+} + H_2O. \quad (9)$$

Eq. (8) describes the complete breakdown of brannerite to a secondary TiO_2 phase and Eq. (9) provides a description of the role of silica in driving the conversion of brannerite to the glass-like Ti–Si–O phase via a dissolution-reprecipitation mechanism. Because it takes on the order of 10 Ma to reach the critical amorphization dose by alpha decay (see following section and Fig. 10), the cumulative alpha decay dose of the brannerite samples investigated in this study may have varied significantly prior to geochemical alteration. Therefore the structures probably ranged from partially crystalline to fully amorphous during alteration, providing an additional thermodynamic driving force via increased stored energy (metastability) of radiation-damaged brannerite. Nevertheless, brannerite appears to be generally resistant to dissolution at low temperatures in relatively oxidizing environments, for example, the samples from Idaho occur in a placer deposit and have survived the weathering and breakdown of their host rocks with minimal dissolution of the original crystals.

6.4. Radiation damage effects

Based on the Th and U contents and either the known age or the chemical U–Pb age determined by SEM-EDX (Tables 1 and 2), the brannerite samples examined in this work have average calculated alpha decay doses of $2–170\times10^{16}$ α/mg. Results obtained from the SRIM simulations using $E_d = 50$ eV and $\rho = 5.096–6.370$ g cm^{-3} (Table 5) indicate that N_d ranges from 651 to 667 displacements per alpha decay event, of which 560–571 are derived from the collision cascade produced by the recoil nucleus (range = 23 nm) and 91–100 are produced by the alpha particle, mainly near the end of the track (range = 13 μm). Thus, any real variation in density will have only a minor effect on the total number of calculated displacements. However, as shown in Table 5, the variation of the threshold displacement energies has a significant effect on the calculated number of displacements; for E_d values increasing from 25 to 100 eV the corresponding N_d values decrease by a factor of about 4, therefore in the absence of experimental or computational data on the threshold displacement energies for brannerite the calculated dpa values will have considerable uncertainty. In this study, we used a value of $N_d = 660$ ($E_d = 50$ eV) as the basis for the dpa calculation in Eq. (4). Note that the N_d value derived from SRIM simulations is much lower than previously assumed for natural oxide minerals. Typically, a value of $N_d = 1500$ or more has been employed in previous studies and this is in part due to the use of lower E_d values of 20–25 eV. For the dose range observed in this study, the corresponding dpa values range from 0.3 to 104.

The current data set for brannerite is shown in Fig. 10. For comparison, natural pyrochlores and zirconolites with ages of 100 Ma or less become amorphous at doses of approximately 1×10^{16} α/mg (Lumpkin and Ewing, 1988; Lumpkin et al., 1994b). Unfortunately, the critical amorphization dose (D_c) cannot be determined from these samples because none of the grains retained crystallinity, even the geologically young samples. However, using literature data for a partially crystalline brannerite from Binntal, Switzerland (Graeser and Guggenheim, 1990), the critical dose appears to be close to $1–2\times10^{16}$ α/mg. There is some uncertainty in this evaluation based upon the assumed age and calculated dose of the French sample, which places a data point for an amorphous sample just below the partially crystalline data point (Fig. 10). One issue here is that the age of the French sample in not well constrained, it may be older and closer to the age of the Swiss samples, which would move the estimated critical dose to a value in the range of $1.3–3.3\times10^{16}$ α/mg.

None of the samples examined by TEM showed the presence of significant crystalline domains of brannerite, even though some of the samples are geologically young. Furthermore, the amphibolite grade thermal event (temperatures of 500–650 °C are typical) experienced by the samples from Crocker's Well was either insufficient to restore crystallinity in these geologically old brannerite samples or the recovery of damage was subsequently erased within the samples due to continued alpha decay damage after the peak of metamorphism.

Table 5
Simulated number of displacements per recoil atom (^{234}U, 80 keV) and alpha particle (^{4}He, 4.5 MeV) in brannerite as a function of displacement energy and density.

	$E_d = 25$ eV			$E_d = 50$ eV			$E_d = 100$ eV		
Density (g cm^{-3})	Recoil	Alpha	Total	Recoil	Alpha	Total	Recoil	Alpha	Total
6.370	1153	211	1364	571	96	667	283	43	326
5.733	1139	217	1356	565	100	665	280	46	326
5.096	1124	199	1323	560	91	651	279	41	320
Average	1139	209	1348	565	96	661	281	43	324

Acknowledgments

This work was performed at the Australian Nuclear Science and Technology Organisation, partly funded under contract with Lawrence Livermore National Laboratory as part of the Plutonium Immobilization Project. We thank R.A. Day and M.G. Blackford for maintenance and calibration of the electron microscopes. Special thanks are due to E. Reusser for organizing field explorations in the Ticino region of south-central Switzerland. We are grateful to C.T. Williams, C.A. Francis, N. Meisser, E. Reusser, and R. Pogson for the loan of museum samples used in this study.

References

Abad-Ortega, M., Hach-Ali, P.F., Martin-Ramos, J.D., Ortega-Huertas, M., 1993. The feldspars of the Sierra Albarrana granitic pegmatites, Cordoba, Spain. The Canadian Mineralogist 31, 185–202.
Ahmed, A.H., Arai, S., Ikenne, M., 2009. Mineralogy and paragenesis of the Co–Ni arsenide ores of Bou Azzer, Anti-Atlas, Morocco. Economic Geology 104, 249–266.
Azor, A., Ballèvre, M., 1997. Low-pressure metamorphism in the Sierra Albarrana area (Variscan Belt, Iberian Massif). Journal of Petrology 38, 35–64.
Bianconi, F., Simonetti, A., 1967. La brannerite e la sua paragenesis nelle pegmatite di Lodrino (Ct. Ticino). Schweizerische Mineralogische und Petrographische Mitteilungen 47, 887–934.
Campana, B., 1954. Absolute age of the uraniferous granite and pre-Cambrian tillite in the Crocker's Well area (Olary district, South Australia). The Australian Journal of Science 16, 240–241.
Campana, B., King, D., 1958. Regional geology and mineral resources of the Olary province. Geological Survey of South Australia, Bulletin 30, 7–50.
Clarke, G.L., Burg, J.P., Wilson, C.J.L., 1986. Stratigraphic and structural constraints on the Proterozoic tectonic history of the Olary block, South Australia. Precambrian Research 34, 107–137.
Colella, M., Lumpkin, G.R., Zhang, Z., Buck, E.C., Smith, K.L., 2005. Determination of the uranium valence state in the brannerite structure using EELS, XPS, and EDX. Physics and Chemistry of Minerals 32, 52–64.
Ewing, R.C., Headley, T.J., 1983. Alpha-recoil damage in natural zirconolite ($CaZrTi_2O_7$). Journal of Nuclear Materials 119, 102–109.
Favreau, G., Dietrich, J.E., Meisser, N., Brügger, J., Haddouch, L.A., Maacha, L., 2007. Famous mineral localities: Bou Azzer, Morocco. The Mineralogical Record 38, 345–407.
Ferris, C.S., Ruud, C.O., 1971. Brannerite: its occurrences and recognition by microprobe. Quarterly of the Colorado School of Mines 66.
Finnie, K.S., Zhang, Z., Vance, E.R., Carter, M.L., 2003. Examination of U valence states in the brannerite structure by near-infrared diffuse reflectance and X-ray photoelectron spectroscopies. Journal of Nuclear Materials 317, 46–53.
Foden, J., Elburg, M.A., Dougherty-Page, J., Burtt, A., 2006. The timing and duration of the Delamerian Orogeny: correlation with the Ross Orogen and implications for Gondwana Assembly. Journal of Geology 114, 189–210.
Gasquet, D., Bertrand, J.-M., Paquette, J.-L., Lehmann, J., Ratzov, G., Guedes, R.A., Tiepolo, M., Boullier, A.-M., Scaillet, S., Nomade, S., 2010. Miocene to Messinian deformation and dhdrothermal activity in a pre-Alpine basement massif of the French western Alps: new U–Th–Pb and argon ages from the Lauzière massif. Bulletin de la Societe Geologique de France 181, 227–241.

Geffroy, J., 1963. La brannerite du filon aurifere de la Gardette (Isere) et sa signification metallogenique. Bulletin de la Societe de France Mineralogie et Cristallographie 86, 129–132.
Graeser, S., Guggenheim, R., 1990. Brannerite from Lengenbach, Binntal (Switzerland). Schweizerische Mineralogische und Petrographisce Mitteilungen 70, 325–331.
Greenhalgh, D., Jefferey, P.M., 1959. A contribution to the pre-Cambrian chronology of Australia. Geochimica et Cosmochimica Acta 16, 39–57.
Headley, T.J., Ewing, R.C., Haaker, R.F., 1981. Amorphous structure of metamict minerals observed by TEM. Nature 293, 449–450.
Hess, F.L., Wells, R.C., 1920. Brannerite, a new uranium mineral. Journal of the Franklin Institute 189, 225–237.
Hewett, D.F., Stone, J., Levine, H., 1957. Brannerite from San Bernardino County, California. American Mineralogist 42, 30–38.
Icenhower, J.P., Strachan, D.M., McGrail, B.P., Scheele, R.D., Rodriguez, E.A., Steele, J.L., Legore, V.L., 2006. Dissolution kinetics of pyrochlore ceramics for the disposition of plutonium. American Mineralogist 91, 39–53.
Ifill, R.O., Cooper, W.C., Clark, A.H., 1966. Mineralogical and process controls on the oxidative acid-leaching of radioactive phases in Elliot Lake, Ontario, uranium ores: II — Brannerite and allied titaniferous assemblages. CIM Bulletin 89, 93–103.
Kampunzu, A.B., Cailtreux, J.L.H., Kamona, A.F., Intiomale, M.M., Melcher, F., 2009. Sediment-hosted Zn–Pb–Cu deposits in the Central African Copperbelt. Ore Geology Reviews 35, 263–297.
Leblanc, M., Billaud, P., 1982. Cobalt arsenide ore bodies related to an upper Proterozoic ophiolite; Bou Azzer (Morocco). Economic Geology 77, 162–175.
Ludwig, K.R., Cooper, J.A., 1984. Geochronology of Precambrian granites and associated U–Ti–Th mineralization, northern Olary province, South Australia. Contributions to Mineralogy and Petrology 86, 298–308.
Lumpkin, G.R., 1992. Analytical electron microscopy of columbite: a niobium-tantalum oxide mineral with zonal uranium distribution. Journal of Nuclear Materials 190, 302–311.
Lumpkin, G.R., Ewing, R.C., 1988. Alpha decay damage in minerals of the pyrochlore group. Physics and Chemistry of Minerals 16, 2–20.
Lumpkin, G.R., Ewing, R.C., 1995. Geochemical alteration of pyrochlore group minerals: pyrochlore subgroup. American Mineralogist 80, 732–743.
Lumpkin, G.R., Ewing, R.C., 1996. Geochemical alteration of pyrochlore group minerals: betafite subgroup. American Mineralogist 81, 1237–1248.
Lumpkin, G.R., Hart, K.P., McGlinn, P.J., Payne, T.E., Gieré, R., Williams, C.T., 1994a. Retention of actinides in natural pyrochlores and zirconolites. Radiochimica Acta 66 (67), 469–474.
Lumpkin, G.R., Smith, K.L., Blackford, M.G., Gieré, R., Williams, C.T., 1994b. Determination of 25 elements in the complex oxide mineral zirconolite by analytical electron microscopy. Micron 25, 581–587.
Oberthür, T., Melcher, F., Henjes-Kunst, F., Gerdes, A., Stein, H., Zimmerman, A., El Ghorfi, M., 2009. Hercynian age of the cobalt-nickel-arsenide-(gold) ores, Bou Azzer, Anti Atlas, Morocco: Re–Os, Sm–Nd, and U–Pb age determinations. Economic Geology 104, 1065–1079.
Pabst, A., 1954. Brannerite from California. American Mineralogist 39, 109–117.
Paul, E., Sandiford, M., Flöttmann, T., 2000. Structural geometry of a thick-skinned fold-thrust belt termination: the Olary Block in the Adelaide Fold Belt, South Australia. Australian Journal of Earth Sciences 47, 281–289.
Perez, B.C., Gonzalez, J., Gonzalez, J., 1991. Los Minerales y la Minería de la Sierra Albarrana y su Entorno. Fundación Enresa, Madrid.
Roberts, S.K., Bourcier, W.L., Shaw, H.F., 2000. Aqueous dissolution kinetics of pyrochlore, zirconolite and brannerite at 25, 50, and 75 °C. Radiochimica Acta 88, 539–543.
Saager, R., Stupp, H.D., 1983. U–Ti phases from Precambrian quartz-pebble conglomerates of the Elliot Lake area, Canada, and the Pongola Basin, South Africa. Tschermaks Mineralogische und Petrographische Mitteilungen 32, 83–102.
Simancas, J.F., Galindo-Zaldívar, J., Azor, A., 2000. Three-dimensional shape and emplacement of the Cardenchosa deformed pluton (Variscan Orogen, southwestern Iberian Massif). Journal of Structural Geology 22, 489–503.
Strachan, D.M., Scheele, R.D., Buck, E.C., Icenhower, J.P., Kozelisky, A.E., Sell, R.L., Elovich, R.J., Buchmiller, W.C., 2005. Radiation damage effects in candidate titanates for Pu disposition: pyrochlore. Journal of Nuclear Materials 345, 109–135.
Strachan, D.M., Scheele, R.D., Buck, E.C., Kozelisky, A.E., Sell, R.L., Elovich, R.J., Buchmiller, W.C., 2008. Radiation damage effects in candidate titanates for Pu disposition: zirconolite. Journal of Nuclear Materials 372, 16–31.
Szymanski, J.T., Scott, J.D., 1982. A crystal structure refinement of synthetic brannerite, UTi_2O_6, and its bearing on rate of alkaline-carbonate leaching of brannerite in ore. The Canadian Mineralogist 20, 271–279.
Thomas, B.S., Zhang, Y., 2003. A kinetic model of the oxidative dissolution of brannerite, UTi_2O_6. Radiochimica Acta 91, 463–472.
Torrealday, H.I., Hitzman, M.W., Stein, H.J., Markley, R.J., Armstrong, R., Broughton, D., 2000. Re–Os and U–Pb dating of the vein-hosted mineralization at the Kansanshi copper deposit, northern Zambia. Economic Geology 95, 1165–1170.
Vance, E.R., Watson, J.N., Carter, M.L., Day, R.A., Begg, B.D., 2001. Crystal chemistry and stabilization in air of brannerite, UTi_2O_6. Journal of the American Ceramic Society 84, 141–144.
Zhang, Y., Hart, K.P., Bourcier, W.L., Day, R.A., Colella, M., Thomas, B., Aly, Z., Jostsons, A., 2001. Kinetics of uranium release from Synroc phases. Journal of Nuclear Materials 289, 254–262.
Zhang, Y., Thomas, B.S., Lumpkin, G.R., Blackford, M., Zhang, Z., Colella, M., Aly, Z., 2003. Dissolution of synthetic brannerite in acidic and alkaline fluids. Journal of Nuclear Materials 321, 1–7.
Zhang, Y., Lumpkin, G.R., Li, H., Blackford, M.G., Colella, M., Carter, M.L., Vance, E.R., 2006. Recrystallization of amorphous natural brannerite through annealing: the effect of radiation damage on the chemical durability of brannerite. Journal of Nuclear Materials 350, 293–300.
Ziegler, J.F., Biersack, J.P., Littmark, U., 2009. The Stopping and Range of Ions in Matter. Pergamon Press, New York.